Biophysical Journal Volume 83 November 2002 2681–2692

Translational Diffusion of Individual Class II MHC Membrane Proteins in Cells

Marija Vrljic,* Stefanie Y. Nishimura,† Sophie Brasselet,† W. E. Moerner,*† and Harden M. McConnell*†

*Biophysics Program and †Department of Chemistry, Stanford University, Stanford, California 94305-5080 USA

ABSTRACT Single-molecule epifluorescence microscopy was used to observe the translational motion of GPI-linked and native I-E^k class II MHC membrane proteins in the plasma membrane of CHO cells. The purpose of the study was to look for deviations from Brownian diffusion that might arise from barriers to this motion. Detergent extraction had suggested that these proteins may be confined to lipid microdomains in the plasma membrane. The individual I-E^k proteins were visualized with a Cy5-labeled peptide that binds to a specific extracytoplasmic site common to both proteins. Single-molecule trajectories were used to compute a radial distribution of displacements, yielding average diffusion coefficients equal to 0.22 (GPI-linked I-E^k) and 0.18 μm^2/s (native I-E^k). The relative diffusion of pairs of proteins was also studied for intermolecular separations in the range 0.3–1.0 μm, to distinguish between free diffusion of a protein molecule and diffusion of proteins restricted to a rapidly diffusing small domain. Both analyses show that motion is predominantly Brownian. This study finds no strong evidence for significant confinement of either GPI-linked or native I-E^k in the plasma membrane of CHO cells.

INTRODUCTION

Properties of the cell plasma membrane have been the focus of many studies. However, quantitative details of membrane inhomogeneity and structure have been elusive. The interest in membrane properties intensified recently after detergent extraction studies suggested that plasma membrane components may not be homogeneously mixed (Brown and London, 1998, 2000; Simons and Toomre, 2000). In addition to biochemical approaches, several microscopic imaging methods have been used to study plasma membrane properties. The methods used include fluorescence recovery after photobleaching (FRAP) (Edidin and Stroynowski, 1991; Thomas et al., 1994; Zhang et al., 1991), single-particle tracking of large structures such as antibodies (Wilson et al., 1996), beads (Kusumi et al., 1993; Sako and Kusumi, 1994; Simson et al., 1995; Smith et al., 1999), or low-density lipoproteins (Ghosh and Webb, 1994) attached to membrane proteins, and single-molecule tracking of fluorescent lipids (Schütz et al., 2000). A nonuniform distribution of different types of lipids as well as proteins within the plasma membrane has led to several proposals for lipid microenvironments. This work is reviewed by Brown and London (1998, 2000), Simons and Toomre (2000), and Anderson (1998). These microenvironments have been referred to as caveolae, rafts, detergent-resistant membranes (DRM), detergent-insoluble glycolipid-enriched complexes (DIG), glycolipid-enriched membranes (GEM), and lipid microdomains. Such microenvironments, which may or may not arise from cytoskeletal influence, are reported to be enriched in cholesterol, sphingomyelin, and saturated lipids, but their detailed structure and composition are unknown. It has been reported that many membrane proteins are permanently localized within lipid microenvironments. These include glycosyl phosphatidylinositol (GPI)-linked proteins that span one leaflet and other membrane proteins that span both leaflets of the plasma membrane. In addition, it has been reported that some proteins can also translocate to lipid microenvironments in response to the initiation of an extracellular signaling pathway.

The presence of microenvironments within the plasma membrane may be detected as deviations from two-dimensional translational Brownian motion (Qian et al., 1991; Saxton and Jacobson, 1997). Several studies of diffusion trajectories of both lipid and protein membrane constituents provide support for the hypothesis of microenvironments in membranes. These measurements have suggested that lipid microdomains have radii of 26 nm (Pralle et al., 2000), 25-50 nm (Suzuki and Sheetz, 2001), 150 nm (Sheets et al., 1997), and 700 nm (Schütz et al., 2000), and that their boundaries are permeable (see above references and Dietrich et al., 2001, 2002). In addition, Dietrich et al. (2002) reported that the presence of microdomains does not depend on temperature in the range 10-37°C and that at least some microdomains are stable and immobile for up to 80 s. Microenvironments arising from either direct binding to cytoskeleton or trapping of proteins in areas "fenced off" by cytoskeleton have radii on the order of 150–350 nm (Sako and Kusumi, 1994; Kusumi et al., 1993).

To probe for putative inhomogeneities in the plasma membrane, we have studied translational diffusion of MHC class II membrane proteins using single-fluorophore imaging techniques (for reviews see Moerner (2002) and Weiss (1999)). These methods have the potential to detect inhomogeneity, as ensemble averaging is avoided. By choosing a labeling protocol that attaches one small fluorophore to a

Submitted April 2, 2002, and accepted for publication July 12, 2002.

Address reprint requests to Harden M. McConnell, Dept. of Chemistry, Stanford University, Stanford, CA 94305-5080. Tel.: 650-723-4571; Fax: 650-723-4943; E-mail: harden@stanford.edu.

Sophie Brasselet's present address is Laboratoire de Photonique Quantique of Moleculaire, Ecole Normale Superieure de Cachan, 94235 Cachan Cedex, France.

0006-3495/02/11/2681/12 $2.00

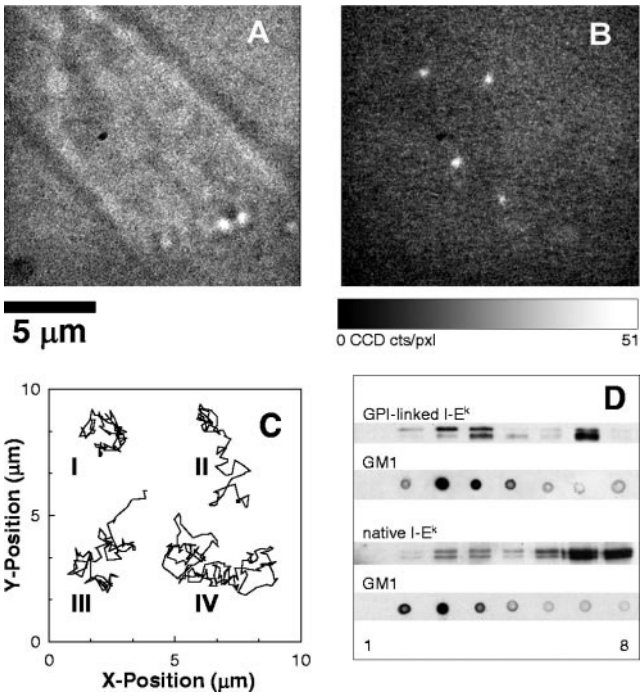

FIGURE 1 Examples of imaging, trajectories, and detergent extractions. (*A*) Bright field image (13 × 13 μm) of the top, center region of an oblong CHO cell. The image shows the outline of the cell running from upper left to lower right, with some internal cellular structures. (*B*) Fluorescence image of the same CHO cell showing spatial distribution of I-E^k proteins on the cell surface (*bright dots*). Spatial distribution of the bright dots changes with time, indicating that fluorescent spots are mobile. Fluorescent spots represent a labeled peptide bound to the protein (see Materials and Methods). (*C*) Examples of characteristic trajectories of GPI-linked (tracks I and II) and native I-E^k (tracks III and IV); coordinates are 100 ms apart. (*D*) Western blots showing localization of GPI-linked and native I-E^k within Triton X-100-resistant parts of the plasma membrane; ~35–50% of GPI-linked and ~5–25% of native I-E^k are found in the Triton X-100-resistant fractions (2–4). Fractions are labeled from top (1) to the bottom of the gradient (8). Only plasma membrane proteins were included in the analysis by biotinylating surface proteins before cell lysis. As a control for the density gradient, the distribution of GM1 is shown for both GPI-linked and native I-E^k, respectively ("dot blots"); ~70% GM1 is found in the Triton X-100-resistant fractions (2–4).

protein, the perturbation caused by the labeling is far smaller than in previous studies. The cost of such an approach is reduced observation time (a few seconds compared to several minutes in other SPT studies). The MHC class II protein system is convenient in that it enables facile *in vitro* labeling of the protein by binding of its labeled peptide ligand. Certain small peptides bind to a specific site, the extracellular peptide-binding groove, on the MHC class II molecules with high specificity. Interactions of peptide ligands with class II MHC molecules have been characterized extensively (see Reay et al., 1994, Marshall et al., 1995, Rabinowitz et al., 1998, and Schmitt et al., 1998). This data base provides control over the extent of labeling of the MHC class II protein and the half-life of the protein-peptide interaction. In this study, a peptide with long dissociation $t_{1/2}$ (>200 h) was used, and it was labeled with a red absorbing and emitting fluorophore to avoid cellular autofluorescence.

The MHC class II proteins studied were two varieties of the I-E^k: a GPI-linked and the native I-E^k. Detergent extraction has linked these proteins with lipid microenvironments (Fig. 1 *D* and Anderson et al., 2000, Hubby et al., 1999). Varma and Mayor (1998) reported that microdomains, sensitive to cholesterol removal, with diameters <70 nm, are present in CHO cells. In addition, FaivreSarrailh et al. (2000) and Hiscox et al. (2002) have reported the presence of detergent-resistant membrane fractions and localization of some membrane proteins within those fractions in CHO cells. The above suggests that lipid microdomains, as defined by detergent-resistance, exist in this cell line. Both GPI-linked and native I-E^k share the same extracytoplasmic domain. However, while native I-E^k is a single-pass membrane protein, GPI-linked I-E^k is lipid-linked, i.e., the cytoplasmic and transmembrane parts of the native I-E^k are replaced by two GPI-linkers that tether it to the outer leaflet of membrane (Wettstein et al., 1991).

The diffusion of individual I-E^k proteins was visualized in CHO cells using a Cy5-labeled MCC 95–103 peptide. The individual trajectories were analyzed in detail to search for possible deviations from Brownian diffusion. To test for possible confinement within moving domains, the relative diffusion of pairs of proteins was also explored, a measurement that can only be obtained from single-particle imaging. These analyses indicate that both GPI-linked and native I-E^k are mobile and diffuse in a fashion that is predominantly consistent with a two-dimensional Brownian motion.

MATERIALS AND METHODS

Cell culture

Chinese hamster ovary (CHO) cells were grown in RPMI 1640 phenol red-free media (Gibco BRL, Grand Island, NY) supplemented with 10% fetal calf serum (HyClone, Logan, UT), 10 mM HEPES (4-(2-hydroxyethyl)-1-piperazineethanesulfonic acid), 1 mM sodium pyruvate, 20 μM 2-mercaptoethanol (2-hydroxy-1-ethanethiol), and 0.1 mM nonessential amino acids, 100 units/ml penicilin, 100 μg/ml streptamycin, 10 μg/ml gentamicin, 0.5 mg/ml geneticin (Gibco BRL), pH 7.4, and 5% carbon dioxide at 37°C. CHO cells transfected with native mouse MHC class II protein, I-E^k (CHO-I-E^k), and CHO cells transfected with I-E^k extracytoplasmic domain fused with glycosylphosphatidylinositol (GPI) linker (CHO-GPI linked I-E^k) were a generous gift of M.M. Davis, and have been previously described (Wettstein et al., 1991). CHO-I-E^k and CHO-GPI-linked I-E^k cells were made by transfecting the original CHO clone, which

was morphologically a mixture of fibroblast and epithelial cells. The measurements were performed on spindly cells with a fibroblast morphology. CHO-K1 cells (ATCC, Manassas, VA) are a subclone with epithelial cell morphology. Cells were grown on a chambered coverglass (Nalge Nunc International, Naperville, IL). To facilitate adhesion of cells, the coverglass was coated with 50 μg/ml fibronectin (human plasma, CalBiochem, San Diego, CA) in phosphate buffered saline (PBS) pH 7.4 (Gibco BRL) for 1 h at room temperature before deposition of cells.

Peptide synthesis

Peptide synthesis, purification, and labeling were performed as described in Schmitt et al. (1998). Briefly, Moth Cytochrome C peptide, MCC 95–103 (IAYLKQATK), was synthesized using standard Fmoc chemistry. The peptide was fluorescently labeled at the N-terminus with Cy5 monofunctional dye (AmershamPharmacia, Piscataway, NJ) and purified by reverse-phase chromatography. Identity and dye/peptide ratio were verified by high-resolution mass spectroscopy. There was one dye moiety per peptide.

Imaging conditions (cells)

Cells were imaged in supplemented RPMI 1640 phenol red-free media with an enzymatic oxygen scavenger system: 1% v/v glucose (Sigma, St. Louis, MO; 500 mg/ml stock), 1% v/v glucose oxidase (Sigma, 5000 U/ml stock), 1% v/v catalase (Sigma, 40000 U/ml stock), and 0.5% v/v 2-mercaptoethanol (Sigma, 14.3 M stock) were added to supplemented RPMI 1640 before imaging. CHO cells can cycle between aerobic and anaerobic metabolism without effects on their viability (data not shown; Rabinowitz, 1998). Imaging was done at 22°C, while treatments with different drugs before imaging were done at 37°C. Cells were labeled by incubation with 0.05–0.1 μg/ml Cy5-MCC 95–103 peptide for 15 min at 37°C. Peptide concentration was adjusted such that a maximum of 0.3 labeled I-E^k molecules/μm^2 were observed, giving a labeling ratio of 1:10^4 labeled-to-unlabeled I-E^k molecules. There are $\sim 10^6$ I-E^k molecules on the cell surface of CHO cells (Vacchino and McConnell, 2001). Properties of I-E^k-MCC 95–103 were extensively characterized elsewhere (Rabinowitz et al., 1998; Reay et al., 1992). Briefly, only one MCC 95–103 peptide binds to one I-E^k MHC class II protein, and the half-life, $t_{1/2,}$ at pH 7.0, 37°C is >200 h. Therefore, the I-E^k-MCC 95–103 complex does not dissociate on the time scale of the imaging.

Antibodies

I-E^k-specific antibody, 14.4.4S, labeled with phycoerythrin at 1:1 ratio (Pharmigen, San Diego, CA), and I-E^k-MCC 95–103-specific antibody, G35-phycoerythrin (generous gift of M. M. Davis), were used to determine whether Cy5-MCC 95–103 binds exclusively to I-E^k proteins on the cell surface, as described below. G35-PE is somewhat cross-reactive with peptide-free I-E^k. The concentration of antibodies was adjusted to yield one fluorescent spot/μm^2. Cells were incubated with antibodies for 20 min at 4°C. Rabbit anti-I-E^k (generous gift of M. M. Davis) was used for Western blots.

Specificity of peptide-I-E^k labeling on the cell surface

The specificity of labeling was established in two ways: 1) the peptide emission in red was superimposed with the emission in green from two antibodies that recognize I-E^k, 14.4.4S-PE, and G35-PE. Red fluorescence from the labeled peptide always coincided with antibody fluorescence in green, indicating that the labeled peptide was associated with I-E^k and did not bind nonspecifically to the plasma membrane (data not shown). 2) Fluorescence from the labeled peptide was absent in the CHO-K1 cells that do not express I-E^k proteins, indicating that Cy5-MCC95-103 peptide binds exclusively to I-E^k, and not to other membrane components (data not shown). A small fraction of fluorescent spots observed on the cells ($\leq$1%) does not originate from labeled peptide. These spots are immobile and fluoresce nonspecifically: they emit when excited with both 633 nm and 532 nm even in the absence of peptide or I-E^k-specific antibodies. By contrast, Cy5-labeled peptide emits only when excited with 633 nm (data not shown). To establish that each fluorescent spot represented one peptide bound to one I-E^k, the fluorescence intensity of a spot was observed as a function of time. The resulting fluorescence intensity profile was clearly characteristic of single-molecule emission; single-step photobleaching to the background after a few seconds (2–10 s) and blinking were observed (data not shown).

Isolation of detergent-resistant membranes

Surface proteins were labeled with biotin (Pierce, Rockford, IL) by incubating 1×10^7 cells with 1 mg/ml Sulfo-NHS-LC-biotin in 1.5 ml of PBS at 4°C for 1 h. Cells were washed of excess biotin, and bovine serum albumin (1 mg/ml) was added to the lysis media. The cells were lysed in 400 μl MNE buffer (Anderson et al., 2000), 0.5% Triton X-100, with protease inhibitors. The lysates were run over 40% (800 μl), 30% (2 ml), 4% (1 ml) sucrose gradient in MNE buffer by centrifugation at 200,000 $\times$ g for 16 h at 4°C. The gradient was fractionated from the top, 500 μl per fraction. Aliquots were incubated with strepavidin-coated beads (Pierce) for 4–8 h at 4°C. Beads were washed, mixed with loading buffer, boiled, and analyzed by SDS-PAGE followed by Western blots. I-E^k protein was detected with rabbit anti-I-E^k. GMI was "dot blotted" and detected with HRP-CT-B (Sigma). Percent protein or GMI in each fraction was determined by densitometer readouts of Western blots and "dot blots." All fractions (including loading fraction) were included in the analysis.

Cytoskeletal disruption

Stock solutions of nocodazole (Sigma, 20 mM stock) and cytochalasin D (Sigma, 1 mg/ml stock solution) were prepared in dimethyl sulfoxide (DMSO). Control cells were treated with an equivalent amount of DMSO alone. For tubulin depolymerization, cells were treated for 30 min at 37°C with 100 μM nocodazole. At this nocodazole concentration tubulin is disrupted after only 5 min of treatment (Huby et al., 1998). For actin depolymerization cells were treated for 30 or 60 min at 37°C with 0.5, 5.0, and 20 μg/ml (1, 10, and 40 μM) cytochalasin D. At a similar range of concentrations others have observed depolymerization of actin filaments (Rotsch and Radmacher, 2000; Stevenson and Begg, 1994). Both drugs were present in the media during imaging.

Experimental apparatus for single-molecule microscopy

The fluorescence imaging of the cells was performed with wide-field epi illumination in an area of $\sim$15 μm $\times$ 15 μm, using an inverted microscope (Eclipse TE300, Nikon, Burlingame, CA). Laser illumination at 633 nm provided an intensity of $\sim$5 kW/cm^2 at the sample plane. The epifluorescence was collected with a 100$\times$ magnification, 1.3 NA, oil-immersion objective (CFI PlanFluor, Nikon) and, for Cy5, imaged through a 645 nm dichroic mirror and a 670 nm band-pass filter (Omega Optical Inc., Brattleboro, VT) on an intensified frame-transfer CCD-camera (I-Pentamax, Roper Scientific, Trenton, NJ). Excitation with 532 nm laser light and a 584 nm band-pass filter and a 545 nm dichroic mirror were used for imaging green fluorescence from antibodies (Omega Optical, Inc.). Images were recorded continuously at a frequency of 10 Hz, fixing the integration time at 100 ms. With these conditions, we obtained a signal-to-background

ratio of 1.6. The average signal without background was 751 ± 206 counts, and the average background was 477 ± 77 counts. The diffraction-limited spot size for immobile particles had a diameter of ~300 nm, while mobile particles had an average diameter of ~500 nm for 100 ms. Beam intensity was adjusted to result in an acceptable signal-to-background ratio while extending the $t_{1/2}$ of the fluorophore. Bright-field illumination from a condenser allowed the direct visualization of the edges of the cells.

Analysis of the trajectories

CHO cells adhere well to the treated glass surface, becoming spindly with dimensions of ~30 × 10 × 5 μm. Thus, the bottom and the top portions of the plasma membrane are parallel to the focal plane of the microscope and can be treated as two-dimensional planes. We have observed similar diffusion of GPI-linked and native I-E^k proteins in the bottom and the top membranes of the cells. However, labeled peptides that were nonspecifically attached to the coverglass were also visible in the images of the bottom membrane. Near the edges of the cell out-of-focal-plane diffusion can occur, and could be detected by an increase in the spot size. Therefore, only single molecules on the upper surface and away from cell edges were included in the analyses. Single-molecule trajectories were mapped by determining the center of mass of the fluorescent spot in each frame with an accuracy of ~±60 nm (diameter of one pixel). This spatial resolution was sufficient in the present experiment since the average displacement of the I-E^k proteins from frame to frame was ~300 nm (from $\langle r^2 \rangle = 4Dt$, where $D = 0.2$ μm^2/s, $t = 0.1$ s (see Results)). The successive (x, y) positions of the proteins on the plane of the cell surface were recorded as a function of time at 100-ms time intervals. These trajectory data were analyzed as described in the Appendix.

RESULTS AND ANALYSIS

To establish the connection between the proteins described here and previous work, membrane extractions were performed and quantified as described above. Approximately 35–50% of GPI-linked and 5–25% of native I-E^k proteins have been found in the Triton X-100-resistant parts of the plasma membrane (Fig. 1 *D* and Hubby et al., 1999; Anderson et al., 2000). For the single-molecule imaging studies, native I-E^k and GPI-linked I-E^k in CHO cells were labeled with a Cy5-labeled MCC (95–103) peptide. One Cy5 was attached per peptide, and the concentration of labeled peptides was adjusted to yield, on average, 0.3 fluorophores per μm^2 of the cell surface. Approximately 0.01% of the ~10^6 I-E^k molecules found in the plasma membrane were labeled. In white light transmission images cells appeared as oblong structures, as shown in Fig. 1 *A*. In the wide-field epifluorescence images, the labeled proteins were visualized as bright, diffraction-limited spots localized on the surface of the cell (Fig. 1 B). The spatial distribution of the fluorescent spots followed a Poisson distribution; non-Poisson clustering at 0.001–0.01% concentration of labeled protein was not observed (data not shown). The *x-y* trajectories of the individual protein molecules were obtained by recording the central position for each of the fluorescent spots as a function of time at 100-ms intervals (Fig. 1 *C*). To ensure that single copies of the I-E^k were analyzed, only fluorescent spots in the central region of the upper cellular plane that showed blinking or one-step bleaching were used to create trajectories. The minimum length of the trajectories used in the radial distribution analysis was 1.1 s (11 frames), and the maximum length (limited by photobleaching) was 10 s. No other selection criteria were applied.

Analyses of single-protein trajectories

Because the I-E^k proteins are imaged in the relatively flat plasma membrane, the spatial trajectories may be compared to that for a two-dimensional Brownian motion. A Brownian motion is described by a characteristic probability distribution of displacements r from some origin, $p(r, i\Delta t)$, where the time lag is $i\Delta t$, i is the time step index, and Δt is the time interval between observations. This distribution has the form of r times a Gaussian centered at the origin, which broadens with time lag with an average mean-square displacement, $\langle r^2 \rangle$, equal to $4D(i\Delta t)$, with D the diffusion coefficient. It is often convenient to consider the cumulative radial distribution function, $P(r, i\Delta t)$, which is the probability of finding the diffusing particle within a radius r from the origin at time lag $i\Delta t$:

$$P(r, i\Delta t) = \int_0^r p(r', i\Delta t)dr' = 1 - \exp\left[-\frac{r^2}{4D(i\Delta t)}\right] \quad (1)$$

Cumulative radial distribution function (CDF) plots for each time lag were constructed using 100 trajectories for GPI-linked I-E^k and 200 trajectories for native I-E^k, and fitted to Eq. 1 to extract an estimate of the mean (apparent) diffusion coefficient for each case. In this analysis, the individuality of the trajectories was disregarded and the combined distribution of all independent displacements from all trajectories at a specific time lag was analyzed (see Appendix). Fig. 2, *A* and *B* presents examples of such fits for both GPI and native I-E^k at a 1.0-s time lag along with residuals. Data for the other time lags are similar to the one shown (data not shown). The residuals indicate the presence of a small systematic deviation from a two-dimensional Brownian motion.

To explore the nature of the observed deviation, the apparent diffusion coefficients were examined as a function of time lag. For a pure two-dimensional Brownian motion, the plot of the apparent diffusion coefficient versus time lag would be characterized by a zero slope, indicating that the diffusion coefficient is constant with time lag, and the mean-squared displacement grows linearly with time lag. The experimental results for both proteins showed a small negative slope (Fig. 2, *C* and *D*). The mean diffusion coefficients were $D = 0.22 \pm 0.031$ μm^2/s for GPI-linked and $D = 0.18 \pm 0.013$ μm^2/s for native I-E^k. The minor downward slope was characterized by the anomalous diffusion parameter, α, which has been used to express the deviation from a two-dimensional Brownian motion. For a

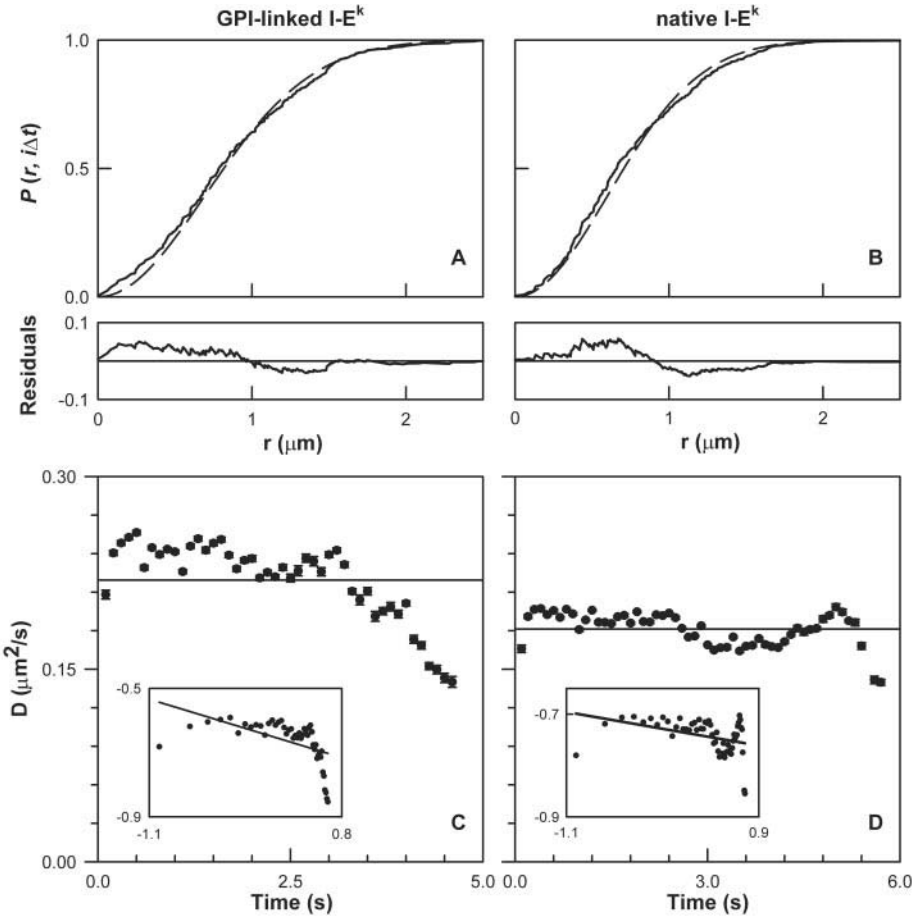

FIGURE 2 Analysis of trajectories by cumulative radial probability distribution. (*A*) One population radial distribution fit exemplified for GPI-linked I-E^k (100 trajectories, from 12 cells) and time lag = 1.0 s. (*B*) Same analysis as in *A* for native I-E^k (200 single trajectories, from 25 cells). The solid line represents the data points, the dashed line represents the least-squares fit to Eq. 1. *Insets:* the residuals of the fits to Eq. 1. (*C*) Apparent diffusion coefficients (·), calculated from radial distribution function fits (Eq. 1), plotted as a function of time lag for GP1-linked I-E^k. The solid line represents the mean value of *D*, $D = 0.22 \pm 0.031$ μm^2/s. Error bars for each *D* represent standard error from the fit to Eq. 1 for each respective time lag. Standard deviation reported for the mean *D* is the standard deviation of the *D* values calculated at each time lag. Maximum depicted time lag is 4.6 s for GPI-I-E^k. Maximum time lag was chosen as the longest time lag to which at least 50 individual trajectories contribute. *Inset:* (log *D* *vs.* log *t*) $\alpha = 0.90 \pm 0.022$, $D_0 = 0.23 \pm 2.4 \times 10^{-3}$ μm^2/s. (*D*) Native I-E^k; all other parameters as in *C*. Maximum depicted time lag is 5.7 s. The mean value of *D* is 0.18 ± 0.013 μm^2/s. *Inset:* $\alpha = 0.97 \pm 0.01$, $D_0 = 0.19 \pm 0.001$ μm^2/s.

two-dimensional Brownian motion $\alpha = 1$ and for anomalous diffusion $0 < \alpha < 1$ ($D = D_0 t^{\alpha-1}$; $\langle r^2 \rangle = 4D_0 t^{\alpha}$) (Saxton, 1994; Smith et al., 1999; Feder et al., 1996). The values for α were found to be $\alpha = 0.90 \pm 0.022$, $D_0 = 0.23 \pm 0.002$ μm^2/s for GPI-linked and $\alpha = 0.97 \pm 0.029$, $D_0 = 0.19 \pm 0.001$ μm^2/s for native I-E^k (Fig. 2 *C* and *D*, *insets*). These values indicate almost negligible deviation from Brownian motion for both native-I-E^k and GPI-linked I-E^k proteins.

To explore further the possibility of deviations from a single Brownian population, two approaches were used. First, the CDF data were fit to a linear combination of terms as in Eq. 1, with two diffusion coefficients and two diffusing population fractions (Schütz et al., 1997). Such fits to our data suggested the presence of a second, slower-diffusing population. On average, the slower population gave a $D_2 \approx 0.14 \pm 0.12$ μm^2/s and constituted $20 \pm 18\%$ of all molecules (data not shown). However, random walks generated by Monte Carlo simulations, with a single diffusion coefficient of $D = 0.2$ μm^2/s, $t - 5$ s (parameters used based on the experimental data), also showed the presence of the second, slow-diffusing population when fitted to the linear combination of Eq. 1. Standard deviations for both the value of the second diffusion coefficient and the fraction assigned to the second diffusing population were of the same order of magnitude as the values themselves ($D_2 \approx 0.13 \pm 0.11$ μm^2/s, $\%D_2 \approx 15 \pm 15$). As indicated above, this was also true for the second diffusion coefficient, D_2, and the fraction assigned to it for the experimental data. In addition, 200 simulated random walks, where 95% had a $D = 0.2$ μm^2/s and 5% had a $D = 0.02$ μm^2/s, yielded $D_2 \approx 0.05 \pm 0.07$ μm^2/s, $\%D_2 \approx 14 \pm 12$ when fitted to the linear combination of Eq 1. In conclusion, for our data, the detection of 5–15% of a second diffusing population using ensemble fits to the linear combination of Eq. 1 is below the fitting threshold. Therefore, this analysis did not show the presence of a distinct second population with a constant diffusion coefficient.

In a second approach, the distribution of apparent diffusion coefficients of the individual trajectories was constructed to test for heterogeneity from molecule to molecule. In Fig. 3, the distribution of apparent diffusion coefficients for individual molecules is shown for native and GPI-linked I-E^k. While many of the GPI-linked I-E^k molecules follow expected distribution (Fig. 3 *A*, *solid lines*, see Appendix and Eq. A1) and show apparent diffusion coefficients clustered around ~ 0.25 μm^2/s, it is clear that a few molecules, $\sim 6\%$, are characterized by slower diffusion ($D \approx 0.02$

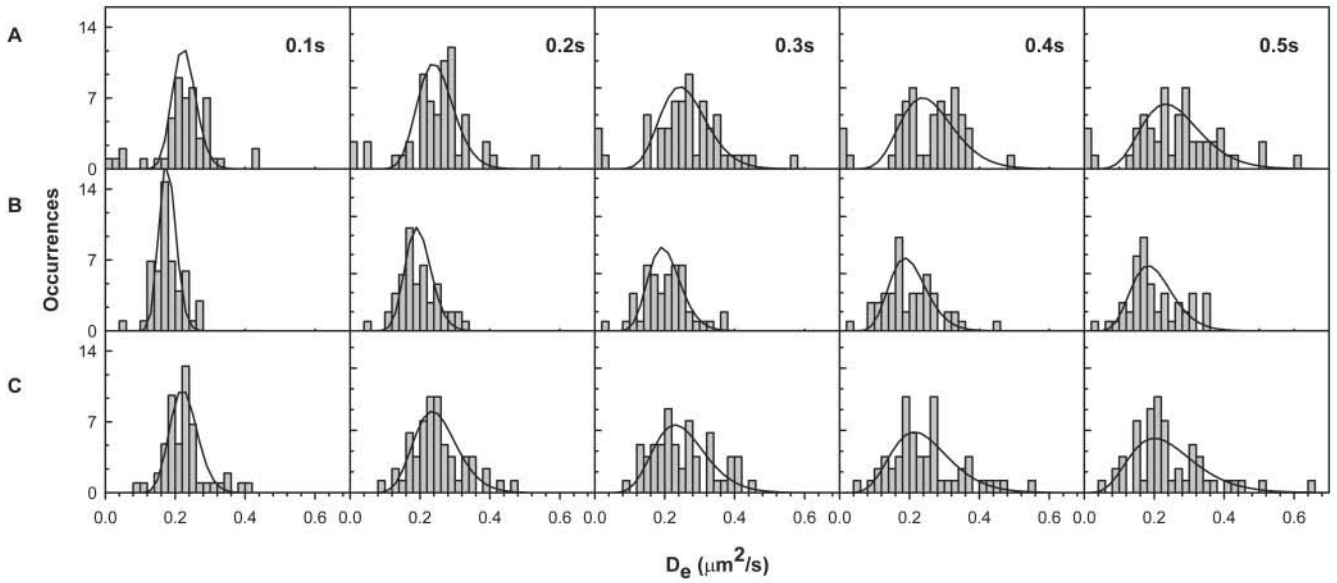

FIGURE 3 Distribution of apparent diffusion coefficients of individual trajectories for different time lags, $i\Delta t$. (*A*) GPI-linked I-E^k. Diffusion coefficients for individual trajectories were estimated as described in the Appendix. The histogram was created from 50 trajectories that lasted ≥4.6 s, but for this analysis the trajectories were all cut to be 4.6 s long. The last shown time lag was chosen such that at least nine displacements were used to estimate D_e. The solid line represents expected distribution of diffusion coefficients for two-dimensional Brownian motion (Eq. A1) with $\langle D_0 \rangle_{\text{for } i\Delta t(0.1-0.5s)} = 0.25 \pm 0.015\ \mu m^2/s$, $N = 4.6s/i\Delta t(s)$. (*B*) Native I-E^k; 51 trajectories, ≥5.7 s long, all cut to be 5.7 s long. $\langle D_0 \rangle_{\text{for } i\Delta t(0.1-0.5s)} = 0.20 \pm 0.010\ \mu m^2/s$, $N = 5.7s/i\Delta t(s)$. All other parameters as in *A*. (*C*) GPI-linked I-E^k; influence of actin depolymerization (40 μM cytochalasin D, 30 min, 37°C); 52 trajectories, ≥3.3 s long, all cut to be 3.3 s long. $\langle D_0 \rangle_{\text{for } i\Delta t(0.1-0.5s)} = 0.24 \pm 0.040\ \mu m^2/s$. $N = 3.3s/i\Delta t(s)$. All other parameters as in *A*, with the exception that for the last shown time lag at least six displacements were used to estimate D_e.

$\mu m^2/s$). However, native I-E^k molecules follow expected distribution (Fig. 3 *B*). This result suggests that the diffusion is predominantly Brownian, with a small fraction of the proteins, ~6% (GPI-linked I-E^k), diffusing with much smaller diffusion coefficients. Of this slow-moving fraction 66% are confined in an area with a radius of ~100 nm (data not shown). This information would have been difficult to obtain without a single molecule experiment.

Relative diffusion of pairs of GPI-linked and native I-E^k proteins

The above radial distribution analysis is informative for the case of protein diffusion within a stationary microdomain, but may fail to describe the combined diffusion of a protein within a microdomain that is itself diffusing. Analysis of the correlation in diffusion between close pairs of single proteins addresses this problem. If two or more particles are trapped within the same microdomain, then the relative distance between the particles should increase more slowly than expected for two independently diffusing particles regardless of whether the microdomain is immobile or mobile. Therefore, we have analyzed the relative motion of pairs of proteins and recorded changes in inter-protein distances as a function of time (Fig. 4).

The distribution of distances between two Brownian particles, each diffusing with diffusion coefficient D, is analyzed as relative motion in a coordinate system in which one particle is fixed at the origin. In this frame of reference, a moving particle has a relative diffusion coefficient $E = 2D$. A useful metric is the probability of finding the second protein within a distance R from the origin at time t, given that the second protein was within some distance ρ_0 from the origin at $t = 0$ (see Appendix and Fig. 6). Time $t = 0$ is defined as the first time the two I-E^k proteins are within 0.3–1.0 μm (ρ_0) of each other. (Due to the diffraction-limited spot size, inter-protein distances <300 nm were not resolvable.) The largest initial separation distance was chosen to be 1.0 μm; however, the molecules were required to be within 1.0 μm of each other only for the first frame. The proteins in the pair were monitored until one of the labeled proteins bleached. Trajectories <0.6 s in length were not considered. To generate a distribution, we applied the following proximity criterion: for the lifetime of the pair, only those times when the inter-protein distance was ~ $2\rho_0$ were scored as positive hits. Any reentry events were counted relative to the first frame of the pair.

Fig. 4 (*A–F*) shows the results of this pair analysis, where the abscissa is the dimensionless time parameter $\varepsilon = 4Et/\rho_0^2$, with t equal to the time lag, ρ_0 equal to the initial separation between the two proteins, and E involves the mean value of diffusion coefficient from Fig. 2 *C* or *D* above. The solid line represents the theoretical cumulative distribution of finding two proteins within $2\rho_0$ of each other

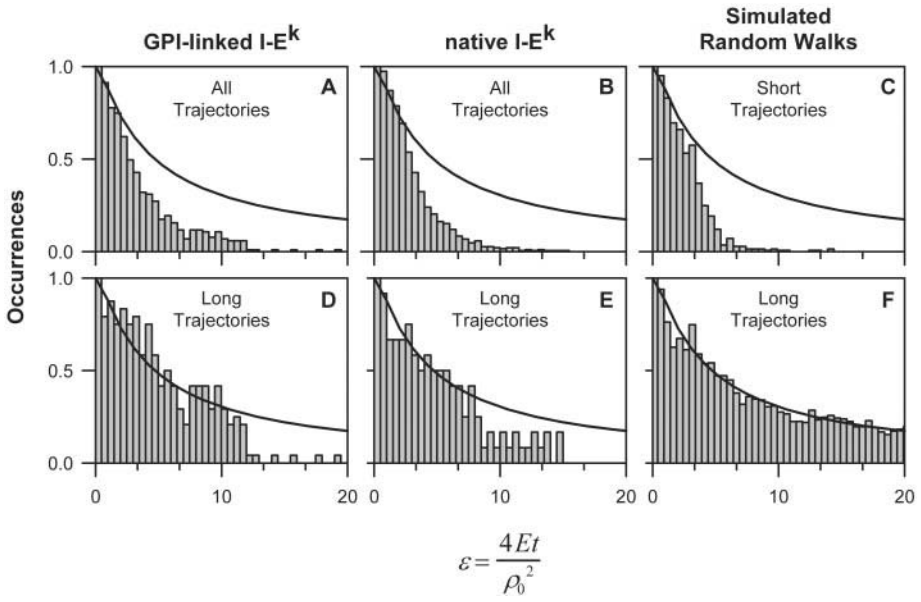

FIGURE 4 Analysis of relative diffusion between pairs of membrane proteins. (*A*) GPI-linked I-E^k. The histogram represents the probability distribution of the data obtained from 74 pairs (from 11 cells). $D = 0.22\ \mu m^2/s$ was used to calculate ε. Pairs with separation distances (ρ_0) between 0.3–1 μm at $t =$ 0 ms were analyzed. The minimum length of analyzed trajectories was 600 ms, the average length of a pair was 1.8 s. Given our mean diffusion coefficients for both native I-E^k and GPI-I-E^k, 600 ms is a mean time required for the distance between two molecules to reach $2\rho_0$ if they started $\rho_0 = 1\ \mu$m apart. The solid line is the plot of Eq. A7. (*B*) Native I-E^k; $D = 0.18\ \mu m^2/s$ was used to calculate ε. For the 96 pairs used, the average length of a pair was 1.5 s (from 7 cells). All other parameters as in *A*. (*C*) Monte Carlo simulation of random walks. One point tracer that begins distance ρ_0 from the origin walks on a square lattice with a diffusion coefficient equal to *E*, with equal probability of moving in any direction on the lattice. Initial separation distances are given by experimental data. $D = 0.2\ \mu m^2/s$, length 2.0 s, 65 pairs. The Solid line is Eq. A7. (*D*) same as *A*, except that all pairs are at least 2 s long (from 8 cells). (*E*) same as *B*, except that all pairs are at least 4 s long (from 3 cells). (*F*) All parameters except for length same as *C*. The length of the 65 pairs was 500 s.

after time *t*, assuming that both proteins diffuse in Brownian fashion with diffusion coefficient *D* (Eq. A7, see Appendix). Considering 74 pairs for GPI-linked and 96 pairs for the native I-E^k protein (Fig. 4, *A* and *B*, respectively), the data follow the theoretical distribution for small ε, but fall below the theoretical curve at larger ε. This effect could indicate that the distance between proteins grows faster than expected and could be the result of the presence of repulsive forces between the proteins. However, the observed effect can also be an artifact of the length of the trajectories, which we illustrate by considering several additional cases. The histogram of ε, satisfying the proximity criterion, created only for pairs that are at least two seconds long, follows the expected distribution out to larger values of ε (Fig. 4, *D* and *E*), suggesting that short trajectories can cause the observed effect. Over the given range of initial separation distances, shorter trajectories contribute predominantly to the occurrences at lower values of ε (ε is a function of initial separation distance and time). Because the histogram is normalized by dividing occurrences at all ε by the number of occurrences at the smallest ε, if the number of occurrences at smaller ε is proportionally larger than the number at larger ε, the whole histogram will deviate from the expected distribution faster (Fig. 4, compare *A* and *D*, *B* and *E*).

To further substantiate these remarks, Monte Carlo simulations of random walks of different lengths were created and the trajectories were analyzed as experimental data (Fig. 4, *C* and *F*). The relative diffusion coefficients and distribution of initial separation distances in the simulations were obtained from GPI-linked and native-I-E^k "pair" data. The random walk simulations show that short, 2.0-s long trajectories follow and then fall below the theoretical curve (Fig. 4 *C*), while long, 500-s trajectories follow the theoretical curve (Fig. 4 *F*), again suggesting that the observed effect can be due to the short length of trajectories. Therefore, we conclude that there is no evidence of correlated diffusion over inter-protein distances between 0.3 and 1.0 μm.

Influence of cytoskeleton

Previous reports have shown that the cytoskeletal network can influence the diffusion of some plasma membrane proteins, and thus the influence of actin and tubulin networks on the diffusion of I-E^k proteins was investigated (Figs. 5 and 3 *C*). Actin and tubulin fibers were depolymerized using cytochalasin D and nocodazole, respectively. Apparent diffusion coefficients of GPI-linked and native I-E^k versus time lag (Fig. 5, *A–D*) show no significant deviation from two-dimensional Brownian motion in the absence of intact actin and tubulin cytoskeletal networks. Mean diffusion coefficients are $D = 0.26 \pm 0.024\ \mu m^2/s$ (GPI-linked) and

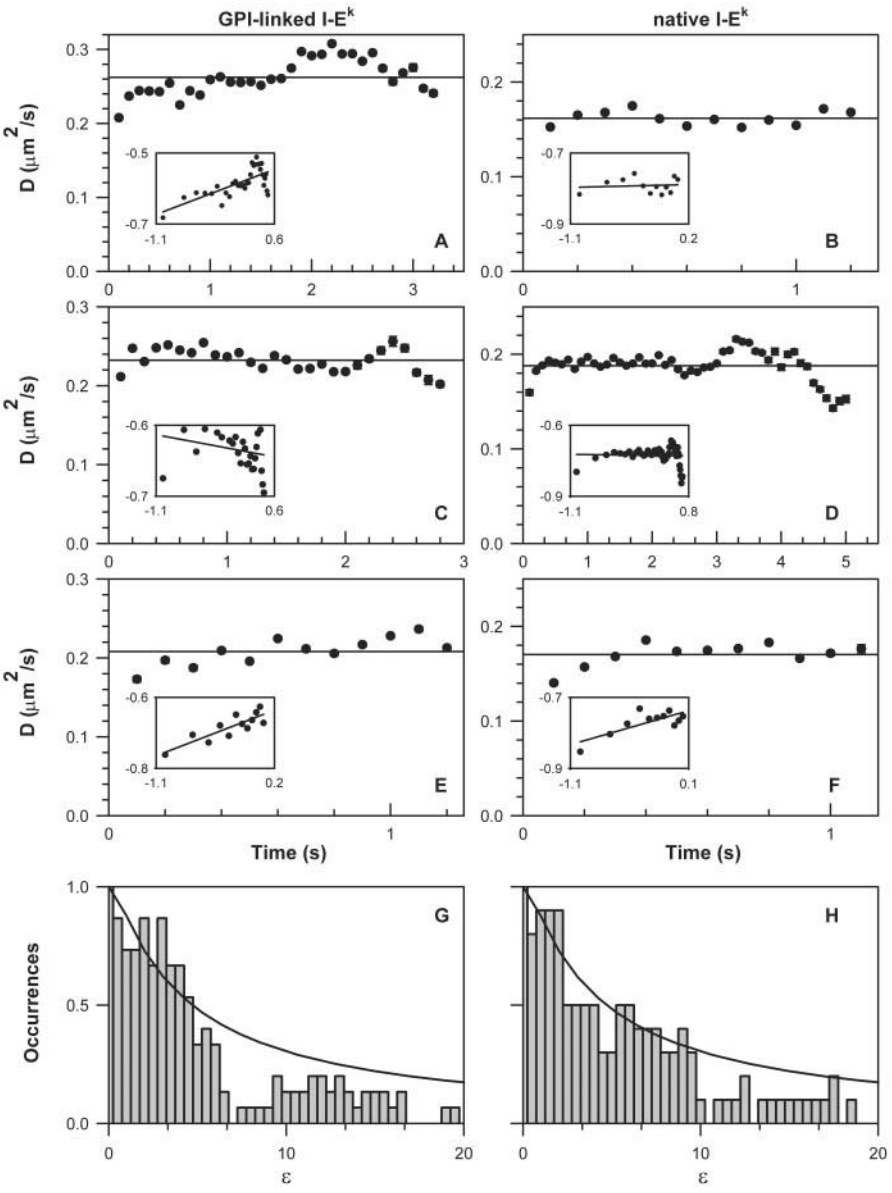

FIGURE 5 Influence of actin and tubulin depolymerization on the diffusion of GPI-linked and native I-E^k proteins. (*A*) Actin disruption for GPI-linked I-E^k. Data are shown for 40 μM cytochalasin D, 30 min, 37°C. The same effect was observed for 10 μM cytochalasin D. Under white light cells are spherical, not spindly, indicating that stress fibers are depolymerized (see Materials and Methods). Shown are diffusion coefficients as a function of time. All other parameters as in Fig. 2 *C;* 104 trajectories were analyzed (from 10 cells) (average length 3.2 s). The mean value of $D = 0.26 \pm 0.024$ μm^2/s. Error bars for each D represent standard error from the fit to Eq. 1 for each respective time lag. *Inset:* $\alpha = 1.07 \pm 0.014$, $D_0 = 0.26 \pm 1.3 \times 10^{-3}$ μm^2/s. (*B*) Actin disruption for native I-E^k. Experimental conditions and fit parameters as in *A;* 52 trajectories (from 9 cells) were analyzed, average length 3.2 s. Mean value of $D = 0.16 \pm 7.8 \times 10^{-3}$ μm^2/s. *Inset:* $\alpha = 1.0 \pm 0.020$, $D_0 = 0.16 \pm 1.4 \times 10^{-3}$ μm^2/s. (*C*) Tubulin disruption for GPI-E^k. Under white light cells are not as spindly as controls and look flattened, suggesting that the tubulin network has depolymerized (see Materials and Methods). Shown are diffusion coefficients as a function of time for 77 trajectories (from 10 cells), average length 2.9 s. All other parameters as in Fig. 2 *C*. Mean value of $D = 0.23 \pm 0.015$ μm^2/s. *Inset:* $\alpha = 0.98 \pm 0.014$, $D_0 = 0.23 \pm 1.2 \times 10^{-3}$ μm^2/s. (*D*) Tubulin disruption for native I-E^k, same as *C;* 123 trajectories were analyzed (from 14 cells), average length 5.1 s. The mean value of $D = 0.19 \pm 0.016$ μm^2/s. *Inset:* $\alpha = 0.99 \pm 0.014$, $D_0 = 0.19 \pm 1.3 \times 10^{-3}$ μm^2/s. (*E*) GPI-linked I-E^k, 4 μl DMSO, 30 min, 37°C. All other parameters as in *A;* 51 trajectories were analyzed (from 6 cells), average length 2.7 s. The mean value of $D = 0.21 \pm 0.018$ μm^2/s. *Inset:* $\alpha = 1.10 \pm 0.019$, $D_0 = 0.22 \pm 0.018$ μm^2/s. (*F*) Native I-E^k, Same as *E;* 37 trajectories were analyzed (from 7 cells), average length 3.3 s. The mean value of $D = 0.17 \pm 0.013$ μm^2/s. *Inset:* $\alpha = 1.08 \pm 0.023$, $D_0 = 0.18 \pm 1.8 \times 10^{-3}$ μm^2/s. (*G*) Actin disruption for GPI-linked I-E^k. Shown is the correlation in diffusion of the "pairs." All parameters as in Fig. 4 *D;* 12 pairs (from 5 cells) longer than 2 s were analyzed. (*H*) Actin disruption for native I-E^k. Experimental conditions and fit parameters as in *G;* 6 pairs (from 2 cells) longer than 3.7 s were analyzed.

$D = 0.16 \pm 7.8 \times 10^{-3}$ $\mu m^2/s$ (native I-E^k) after actin and $D = 0.23 \pm 0.015$ $\mu m^2/s$ (GPI-linked) and $D = 0.19 \pm 0.016$ $\mu m^2/s$ (native I-E^k) after tubulin depolymerization. The extracted α parameters are $\alpha = 1.07 \pm 0.014$ (GPI-linked) and $\alpha = 1.0 \pm 0.020$ (native I-E^k) after actin and $\alpha = 0.98 \pm 0.014$ (GPI-linked) and $\alpha = 0.99 \pm 0.014$ (native I-E^k) after tubulin depolymerization (Fig. 5, *insets* in *A–D*). Fig. 5, *E* and *F* show the effect of DMSO, the solvent used to dissolve cytochalasin D, and nocodazole: $D = 0.21 \pm 0.018$ $\mu m^2/s$, $\alpha = 1.10 \pm 0.019$, $D_0 = 0.22 \pm 0.018$ $\mu m^2/s$ (GPI-linked I-E^k), $D = 0.17 \pm 0.013$ $\mu m^2/s$, $\alpha = 1.08 \pm 0.023$, $D_0 = 0.18 \pm 1.8 \times 10^{-3}$ $\mu m^2/s$ (native I-E^k).

Although these ensemble fits did not show an influence of actin and tubulin depolymerization on the diffusion of GPI-linked and native I-E^k proteins, histograms of diffusion coefficients for GPI-linked I-E^k after actin depolymerization show the absence of slow-diffusing molecules (Fig. 3 *C*), while histograms of diffusion coefficients after tubulin depolymerization still show the presence of the slow-diffusing molecules (data not shown). Histograms of diffusion coefficients of native I-E^k after actin and tubulin depolymerization still follow the expected distribution (data not shown).

Furthermore, analysis of the diffusion of pairs of GPI-linked and native I-E^k proteins after actin disruption show that the data fall below the expected distribution at larger ε in the same way as in the presence of intact cytoskeletal network (compare Fig. 4, *D* and *E* with Fig. 5, *G* and *H*; data for tubulin are similar and are not shown). Therefore, we conclude that actin and tubulin cytoskeletal networks do not significantly influence the translational diffusion of GPI-linked and native I-E^k in CHO cells.

DISCUSSION

In this work we have studied the lateral diffusion of individual molecules of the MHC class II proteins I-E^k, to which a fluorescently labeled MCC 95–103 peptide was specifically bound. The purpose of the study was to determine whether the protein motion conforms to random two-dimensional Brownian diffusion. A more general goal was to determine whether any aspect of the observed protein motion reflects topographical restraints, such as, for example, those that might arise from confining domains with impermeable barriers, or binding to other proteins. There exists a large amount of theoretical literature on the effects of such topologically static barriers on protein diffusion (Saxton, 1993-1995, 1997). In our experiments we have considered not only static barriers, but also a mobile barrier, as might be provided by a diffusing lipid domain in which the protein is confined.

We have found no large deviation of the two-dimensional motion of both GPI-linked and native I-E^k from Brownian diffusion. This holds for essentially all of the labeled proteins for time periods in the range of 2–10 s, the lifetimes of the fluorescent tag before bleaching. Given our observed diffusion coefficients on the order of 0.2 $\mu m^2/s$, this signifies that there are no static impermeable barriers characterized by "cages" with areas in the range of 0.01 to 4.0 μm^2. The lower limit is based on the pixel size of 60 nm. The upper limit was calculated using $\langle r^2 \rangle = 4Dt$, where $t = 5$ s and $D = 0.2$ $\mu m^2/s$. If we use a conservative estimate based on the method of Saxton (1993), then the upper limit would have an area of 0.3 μm^2.

The random diffusion of an individual protein does not preclude the presence of impermeable diffusion barriers if the barriers themselves also diffuse. For this reason we studied the relative diffusion of pairs of proteins, particularly proteins close to one another. In this case we again observed nearly Brownian motion for pairs of proteins separated by distances in the range of 0.3–1.0 μm for times up to 3 s. Thus pairs of proteins cannot be restricted to small, freely diffusing domains with diameters in this range. Our results certainly do not rule out static barriers with areas larger than 0.3–4.0 μm^2 or domains with permeable boundaries.

We note that Fig. 2, *C* and *D* do show that at longer times there is a 20–40% drop-off in apparent diffusion coefficient that is possibly a deviation from random motion. Also, the measured distribution of diffusion coefficients in Fig. 3 shows that some molecules move more slowly than expected (~6% for GPI-linked I-E^k). This slow-moving fraction seems to be actin-related.

Saxton (1995) has shown how static membrane obstacles, or cages with impermeable or partially permeable barriers, can lead to a drop-off in apparent diffusion coefficients at longer times. In addition, a decrease in observed diffusion coefficient with larger measurement times may also occur if every protein undergoes transitions between a "free" and a "bound" state, where in the "bound" state the protein is associated with another protein(s) or large structure, such as caveolae. In this case, measurements at short times would show two diffusion coefficients, whereas measurements at longer times would show a single, average diffusion coefficient. Attempts to reliably analyze the data in this fashion were not possible, as described in the Results section.

The diffusion coefficients found here, 0.18 $\mu m^2/s$ for native I-E^k and 0.22 $\mu m^2/s$ for GPI-linked I-E^k, are close to one another, even though the GPI-linked I-E^k spans only half the bilayer. In analyzing the relationship one should note that the GPI-linker in GPI-linked I-E^k involves two GPI links that are ~15 Å apart.

These observed diffusion coefficients are approximately 10 times smaller than those reported for labeled phospholipids in plasma membranes (Jacobson et al., 1987). Diffusion coefficients reported for other MHC class II proteins at room temperature are in the wide range of $0.1 \times 10^{-4} - 0.4$ $\mu m^2/s$ (Wilson et al., 1996; Wade et al., 1989; Griffith et al., 1988; Munnelly et al., 2000). Our reported diffusion coefficients for GPI-linked and native I-E^k are similar to the diffusion coefficients, at room temperature, found for GPI-

linked proteins Thy-1, PLAP, and Ly6E ($D \approx 0.24-0.28$ $\mu m^2/s$), and for transmembrane proteins Thy-G, PLAP-G, and Ly6E-D^b ($D \approx 0.12-0.17$ $\mu m^2/s$) (Zhang et al., 1991). In addition, the same researchers reported that changing the mode of anchorage from lipid to peptide reduced lateral diffusion by less than a factor of two, similar to our finding. Our measured values are also close to the diffusion coefficient reported for nonspecifically labeled integral membrane proteins in red blood cell tethers, 0.15 $\mu m^2/s$ (Berk and Hochmuth, 1992) and rhodopsin, 0.35–0.39 $\mu m^2/s$ (Poo and Cone, 1974).

Reported diffusion coefficients for some proteins at room temperature are 10-100-fold lower than the diffusion coefficients reported here (Smith et al., 1999; Simson et al., 1998; Wilson et al., 1996; Berk and Hochmuth, 1992). This large range of values reported for protein diffusion has been attributed to interactions with the cytoskeleton, but may also suggest that interaction of protein with local lipid environment may be sensitive to different cell types and temperature. Based on the data in Fig. 5, we conclude that cytoskeletal proteins have no large effect on diffusion of GPI-linked and native I-E^k in CHO cells, which is in agreement with the observation that truncations of cytoplasmic ends of both α and β chains of MHC class II I-A^k molecules have little effect on lateral diffusion of I-A^k molecules (Griffith et al., 1988; Munnelly et al., 2000). Finally, none of the previous studies have visualized the motion of the transmembrane protein by using a single small fluorophore attached to a native peptide ligand. It is possible that the low level of perturbation in our studies enables freer diffusion of the protein.

Detergent extraction of both GPI-linked and native I-E^k MHC class II molecules shows some "detergent resistant" fraction of the sort previously associated with "lipid rafts." This detergent resistance in no way proves an association of the resistive molecules when present in the plasma membrane, but does suggest this possibility. It thus remains to be determined whether the lipid molecules in this fraction somehow affect diffusion of these proteins.

APPENDIX

Radial distribution

For a given time lag, $i\Delta t$, displacements, r, were determined for independent pairs of points i time steps (Δt) apart for each trajectory (Saxton, 1997). Displacement values were pooled and a plot of the cumulative probability distribution, $P(r, i\Delta t)$, was constructed by counting the fraction of displacements with values $\leq r$. These cumulative probability distribution plots were fit to the radial distribution function in Eq. 1. For the calculation of average diffusion coefficient for all trajectories, all displacement values from all trajectories were pooled.

The largest time lag used to estimate diffusion coefficient was chosen such that at least 50 displacements (=50 trajectories) contribute to the cumulative distribution plot, because random walk simulations suggested that fits of Eq. 1 to $P(r, i\Delta t)$ plots constructed using <10 displacements yield diffusion coefficients lower than the true value (data not shown) due to a fitting artifact. While theoretically Eq. 1 asymptotically approaches 1, experimentally the $P(r, i\Delta t)$ plot reaches 1 at the largest observed displacement value. When $P(r, i\Delta t)$ is constructed from a large number of displacements the weight of the largest value is small, and the estimated diffusion coefficients are close to their true value. However, when $P(r, i\Delta t)$ is constructed from a small number of displacements (<10), the largest displacement carries much more weight, causing the estimated diffusion coefficients to be lower than their true value.

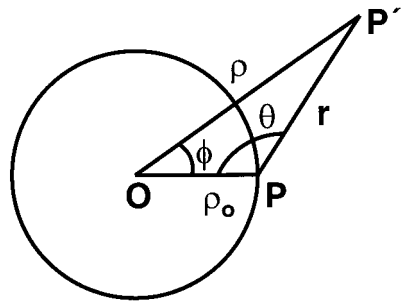

FIGURE 6 Correlated diffusion between two particles is represented by a model in which, at time $t = 0$, one particle is "fixed" at the origin (O) and remains fixed at the origin. The second particle remains mobile and is at P at time $t = 0$, distance ρ_0 from O. The mobile particle is at P′ at some later time t; r is displacement of the mobile particle after time t relative to its starting point (P). ρ is the distance between the stationary particle and mobile particle after time t. ϕ is the angle between vectors OP and OP′.

Probability distribution of diffusion coefficients for Brownian walk

This distribution was derived from the probability distribution of mean square displacements, $p(\langle r^2\rangle)d\langle r^2\rangle$ (Qian et al., 1991; Saxton, 1997), by changing variables using $\langle r^2\rangle = 4D_e i\Delta t$:

$$p(D_e)dD_e = \frac{1}{(N-1)!}\cdot\left(\frac{N}{D_0}\right)^N\cdot(D_e)^{N-1}\cdot\exp\left(\frac{-ND_e}{D_0}\right)\cdot dD_e \qquad \text{(A1)}$$

where $N = N_{total}/i\Delta t$, N_{total} = length of trajectory, $i\Delta t$ = time lag, D_0 = true mean diffusion coefficient, D_e = apparent or experimental diffusion coefficient for an individual trajectory. Because the number of independent pairs, N, needs to be uniform for all trajectories, the tracks were cut such that the first N_{total} points from any trajectory were included in the analysis. For calculation of D_e for an individual trajectory, the mean square displacement for a given time lag was calculated by averaging over independent pairs. Then $D_e = \langle r^2\rangle/4i\Delta t$. Thus calculated D_e values for individual trajectories were used to create histograms of diffusion coefficients for respective time lags. Histograms were normalized by dividing by the total number of trajectories. To plot Eq. A1, the arithmetic mean of D_e values from all trajectories, for a respective time lag, was used as an estimate for D_0.

Relative diffusion between two proteins

The goal is to find a cumulative distribution function for the distances between two Brownian particles diffusing with the same diffusion coefficient, D. For this purpose it is convenient to adopt a frame of reference in which one of the particles is fixed at O (see Fig. 6) and the other is mobile.

In this reference frame, the moving particle has a relative diffusion constant E that is equal to $2D$. The distribution of distances between the two particles is described by the probability that the moving particle starting at position P a distance ρ_0 from the stationary particle at time $t = 0$ will be found at point P′, distance ρ at time t. Diffusion of the moving particle is described by two-dimensional probability density:

$$p(r, t, \theta) = \frac{1}{4\pi Et} \exp\left[- \frac{r^2}{4Et} \right] \tag{A2}$$

Here r is the displacement of the moving particle from its initial position, θ is the angle of the displacement, and t is the time lag.

The basic concept is that we have a probability density function centered at the initial position of the moving particle and we wish to construct a density function centered on the fixed particle (origin). The position of the moving particle is expressed in terms of coordinates relative to the fixed particle, i.e., express r and θ in terms of ρ and ϕ. The angular coordinate θ does not appear in Eq. A2, and can be ignored. The other coordinates are related by:

$$r^2 = \rho_0^2 + \rho^2 - 2\rho_0\rho \cos \phi \tag{A3}$$

By substituting Eq. A3 into Eq. A2 it follows that the probability density of finding the mobile particle at some point P′(ρ, ϕ) at time t is:

$$p(\rho, \phi, t) = - \frac{1}{4\pi Et} \exp\left(- \frac{(\rho_0^2 + \rho^2 - 2\rho_0\rho\cos\phi)}{4Et} \right) \tag{A4}$$

The probability of finding the mobile particle within a distance R of the fixed particle at time t is then:

$$P(\rho \le R, t) = \int_0^R d\rho \int_0^{2\pi} \frac{1}{4\pi Et} \times \exp\left[\frac{-(\rho^2 + \rho_0^2 - 2\rho\rho_0 \cos \phi)}{4Et} \right] \rho d\phi \tag{A5}$$

where ρ_0 is the separation distance between the particles at $t = 0$. The integral over ϕ is given in Carslaw and Jaeger (1959, p. 259) and Abramowitz and Stegun (1965, Eq. 9.6.19). Using that solution and defining dimensionless variables $\varepsilon = 4Et/{\rho_0}^2$, $\rho' = \rho/\rho_0$, and $R' = R/\rho_0$ yields:

$$P(\rho' \le R', t) = \int_0^{R'} \frac{2}{\varepsilon} \exp\left[\frac{-(\rho'^2 + 1)}{\varepsilon} \right] I_0\left[\frac{2\rho'}{\varepsilon} \right] \rho' d\rho' \tag{A6}$$

where I_0 is the zeroth order modified Bessel function of the first kind. The cumulative distribution function $P(\rho' \le R', t)$ depends on ρ_0 only through the scaling parameter ε.

For the particular case discussed in the Results, we apply the proximity criterion that the two particles are within a distance $R = 2\rho_0$ of each other at time t, yielding the desired result:

$$P(\rho' \le 2, t) = \int_0^2 \frac{2}{\varepsilon} \exp\left[\frac{-(1 + \rho'^2)}{\varepsilon} \right] I_0\left[\frac{2\rho'}{\varepsilon} \right] \rho' d\rho' \tag{A7}$$

This integration was performed numerically to produce the smooth curves in Fig. 4 and Fig. 5, *G* and *H*.

The authors gratefully acknowledge E. J. G. Peterman for creating tracking macros, T. G. Anderson, U. Gubler, and M. P. Belmares for useful discussions, and L. Wu for generously sharing antibodies.

This work was supported in part by Grant 5R01AI13587-26 from the National Institutes of Health (to H.M.M.) and in part by Grant 9816947 from the National Science Foundation (to W.E.M.).

REFERENCES

Abramowitz, M., and I. A. Stegun. 1965. Handbook of mathematical functions. Dover Publications, Inc., New York.

Anderson, R. G. W. 1998. The caveolae membrane system. *Annu. Rev. Biochem.* 67:199–225.

Anderson, H. A., E. M. Hiltbold, and P. A. Roche. 2000. Concentration of MHC class II molecules in lipid rafts facilitates antigen presentation. *Nature Immunol.* 1:156–162.

Berk, D. A., and R. M. Hochmuth. 1992. Lateral mobility of integral proteins in red blood cell tethers. *Biophys. J.* 61:9–18.

Brown, D. A., and E. London. 1998. Functions of lipid rafts in biological membranes. *Annu. Rev. Cell & Dev. Bio.* 14:111–136.

Brown, D. A., and E. London. 2000. Structure and function of sphingolipid- and cholesterol-rich membrane rafts. *J. Biol. Chem.* 275: 17221–17224.

Carslaw, H. S., and J. C. Jaeger. 1959. Conduction of Heat in Solids. Oxford University Press, London.

Dietrich, C., Z. N. Volovyk, M. Levi, N. L. Thompson, and K. Jacobson. 2001. Paritioning of Thy-1,GM1, and cross-linked phospholipid analogs into lipid rafts reconstituted in supported model membrane monolayers. *Proc. Natl. Acad. Sci. USA.* 98:10642–10647.

Dietrich, C., B. Yang, T. Fujiwara, A. Kusumi, and K. Jacobson. 2002. Relationship of lipid rafts to transient confinement zones detected by single particle tracking. *Biophys. J.* 82:274–284.

Edidin, M., and I. Stroynowski. 1991. Differences between the lateral organization of conventional and inositol phospholipid anchored membrane proteins. A further definition of micrometer scale membrane domains. *J. Cell Biol.* 112:1143–1150.

FaivreSarrailh, C., F. Gauthier, N. DenishenkoNehrbass, A. LeBivic, G. Rougon, and J. A. Girault. 2000. The glycosylphosphatidyl inositol-anchored adhesion molecule F3/contactin is required for surface transport of paranodin/contactin-assosiated protein (caspr). *J. Cell Biol.* 149: 491–501.

Feder, T. J., I. Brust-Mascher, J. P. Slattery, B. Baird, and W. W. Webb. 1996. Constrained diffusion of immobile fraction on cell surfaces: a new interpretation. *Biophys. J.* 70:2767–2773.

Ghosh, R. N., and W. W. Webb. 1994. Automated detection and tracking of individual and clustered cell surface low density lipoprotein receptor molecules. *Biophys. J.* 66:1301–1318.

Griffith, I. J., Z. Ghogawala, N. Nabavi, D. E. Golan, A. Myer, D. J. McKean, and L. H. Glimcher. 1988. Cytoplasmic domain affects membrane expression and function of Ia molecule. *Proc. Natl. Acad. Sci. USA.* 85:4847–4851.

Hiscox, S., M. B. Hallett, B. P. Morgan, and C. W. van der Berg. 2002. GPI-anchored GFP signals Ca^{2+} but is homogeneously distributed on the cell surface. *Biochem. Biophys. Res. Commun.* 293:714–721.

Hubby, R. D. J., R. J. Dearman, and I. Kimber. 1999. Intracellular phosphotyrosine induction by major histocompatibility complex class II requires co-aggregation with membrane rafts. *J. Biol. Chem.* 274: 22591–22596.

Huby, R. D. J., A. Weiss, and S. C. Ley. 1998. Nocodazole inhibits signal transduction by the T cell antigen receptor. *J. Biol. Chem.* 273: 12024–12031.

Jacobson, K., A. Ishihara, and R. Inman. 1987. Lateral diffusion of proteins in membranes. *Annu. Rev. Physiol.* 49:163–175.

Kusumi, A., Y. Sako, and M. Yamamoto. 1993. Confined lateral diffusion of membrane receptors as studied by single particle tracking (nanovid

microscopy). Effects of calcium-induced differentiation in cultured epithelial cells. *Biophys. J.* 65:2021–2040.

Marshall, K. W., K. J. Wilson, J. Liang, A. Woods, D. Zaller, and J. B. Rothbard. 1995. Prediction of peptide affinity to HLA DRB1*0401. *J. Immunol.* 154:5927–5933.

Moerner, W. E. 2002. A dozen years of single-molecule spectroscopy in physics, chemistry and biophysics. *J. Phys. Chem. B.* 106:910–927.

Munnelly, H. M., C. J. Brady, G. M. Hagen, W. F. Wade, D. A. Roess, and B. G. Barisas. 2000. Rotational and lateral dynamics of I-A^k molecules expressing cytoplasmic truncations. *Int. Immunol.* 12:1319–1328.

Poo, M., and R. A. Cone. 1974. Lateral diffusion of rhodopsin in the photoreceptor membrane. *Nature.* 247:438–441.

Pralle, A., P. Keller, E. L. Florin, K. Simons, and J. K. H. Horber. 2000. Sphingolipid-cholesterol rafts diffuse as small entities in the plasma membrane of mammalian cells. *J. Cell Biol.* 148:997–1007.

Qian, H., M. P. Sheetz, and E. L. Elson. 1991. Single particle tracking. Analysis of diffusion and flow in two-dimensional systems. *Biophys. J.* 60:910–921.

Rabinowitz, J. D. 1998. Potentiometric measurement of intracellular redox activity. *J. Am. Chem. Soc.* 120:2464–2473.

Rabinowitz, J. D., M. Vrljic, P. M. Kasson, J. J. Boniface, M. M. Davis, and H. M. McConnell. 1998. Formation of a highly peptide-receptive state of class II MHC. *Immunity.* 9:699–709.

Reay, P. A., R. M. Kantor, and M. M. Davis. 1994. Use of global amino acid replacements to define the requirements for MHC binding and T cell recognition of moth cytochrome c (93–103). *J. Immunol.* 152: 3946–3957.

Reay, P. A., D. A. Wettstein, and M. M. Davis. 1992. pH dependance and exchange of high and low responder peptides binding to class II MHC molecule. *EMBO J.* 11:2829–2839.

Rotsch, C., and M. Radmacher. 2000. Drug-induced changes of cytoskeletal structure and mechanics in fibroblasts: an atomic microscopy study. *Biophys. J.* 78:520–535.

Sako, Y., and A. Kusumi. 1994. Compartmentalized structure of the plasma membrane for receptor movements as revealed by nanometer-level motion analysis. *J. Cell Biol.* 125:1251–1264.

Saxton, M. J. 1993. Lateral diffusion in an archipelago Single-particle diffusion. *Biophys. J.* 64:1766–1780.

Saxton, M. 1994. Anomalous diffusion due to obstacles: a Monte Carlo study. *Biophys. J.* 66:394–401.

Saxton, M. J. 1995. Single-particle tracking: effects of corrals. *Biophys. J.* 69:389–398.

Saxton, M. J. 1997. Single-particle tracking: the distribution of diffusion coefficients. *Biophys. J.* 72:1744–1753.

Saxton, M. J., and K. Jacobson. 1997. Single-particle tracking: applications to membrane dynamics. *Annu. Rev. Biophys. Biomol. Struct.* 26: 373–399.

Schmitt, L., J. J. Boniface, M. M. Davis, and H. M. McConnell. 1998. Kinetic isomers of a class II MHC-peptide complex. *Biochemistry.* 37:17371–17380.

Schütz, G. J., G. Kada, V. P. Pastushenko, and H. Schindler. 2000. Properties of lipid microdomains in muscle cell membrane visualized by single molecule microscopy. *EMBO J.* 19:892–901.

Schütz, G. J., H. Schindler, and T. Schmidt. 1997. Single-molecule microscopy on model membranes reveals anomalous diffusion. *Biophys. J.* 73:1073–1080.

Sheets, E. D., G. M. Lee, R. Simson, and K. Jacobson. 1997. Transient confinement of a glycosylphosphatidylinositol-anchored protein in the plasma membrane. *Biochemistry.* 36:12449–12458.

Simons, K., and D. Toomre. 2000. Lipid rafts and signal transduction. *Nature (Mol. Cell Biol.).* 1:31–39.

Simson, R., E. D. Sheets, and K. Jacobson. 1995. Detection of temporary lateral confinement of membrane proteins using single-particle tracking analysis. *Biophys. J.* 69:989–993.

Simson, R., B. Yang, S. E. Moore, P. Doherty, F. S. Walsh, and K. A. Jacobson. 1998. Structural mosaicism on the submicron scale in the plasma membrane. *Biophys. J.* 74:297–308.

Smith, P. R., I. E. G. Morrison, K. M. Wilson, N. Fernandez, and R. J. Cherry. 1999. Anomalous diffusion of major histocompatibility complex class I molecules on HeLa cells determined by single particle tracking. *Biophys. J.* 76:3331–3344.

Stevenson, B. R., and D. A. Begg. 1994. Concentration-dependent effects of cytochalasin D on tight junctions and actin filaments in MDCK epithelial cells. *J. Cell Sci.* 107:367–375.

Suzuki, K., and M. P. Sheetz. 2001. Binding of cross-linked glycosylphosphatidylinositol-anchored proteins to discrete actin-associated and cholesterol-dependent domains. *Biophys. J.* 81:2181–2189.

Thomas, J. L., D. Holowka, B. Baird, and W. W. Webb. 1994. Large scale co-aggregation of fluorescent lipid probes with cell surface proteins. *J. Cell Biol.* 125:795–802.

Vacchino, J. F., and H. M. McConnell. 2001. Peptide binding to active class II MHC molecules on the cell surface. *J. Immunol.* 166: 6680–6685.

Varma, R., and S. Mayor. 1998. GPI-anchored proteins are organized in submicron domains at the cell surface. *Nature.* 394:798–801.

Wade, W. F., J. H. Freed, and M. Edidin. 1989. Translational diffusion of class II major histocompatibility complex molecules is constrained by their cytoplasmic domains. *J. Cell Biol.* 109:3325–3331.

Weiss, S. 1999. Fluorescence spectroscopy of single biomolecules. *Science.* 283:1676–1683.

Wettstein, D. A., J. J. Boniface, P. A. Reay, H. Schild, and M. M. Davis. 1991. Expression of a class II major histocompatibility complex (MHC) heterodimer in a lipid-linked form with enhanced peptide/soluble MHC complex formation at low pH. *J. Exp. Med.* 174:219–228.

Wilson, K. M., I. E. G. Morrison, P. R. Smith, N. Fernandez, and R. J. Cherry. 1996. Single particle tracking of cell surface HLA-DR molecules using R-phycoerythrin-labeled monoclonal antibodies and fluorescence digital imaging. *J. Cell Sci.* 109:2101–2109.

Zhang, F., B. Crise, B. Su, Y. Hou, J. K. Rose, A. Bothwell, and K. Jacobson. 1991. Lateral diffusion of membrane-spanning and glycosylphosphatidylinositol-linked proteins: toward establishing rules governing the lateral mobility of membrane proteins. *J. Cell Biol.* 115: 75–84.